



1 **Quality assessment of Second-generation Global Imager**
2 **(SGLI)-observed cloud properties using SKYNET surface**
3 **observation data**

4 Pradeep Khatri¹, Tadahiro Hayasaka¹, Hitoshi Irie², Husi Letu³, Takashi Y. Nakajima⁴, Hiroshi
5 Ishimoto⁵, and Tamio Takamura²

6
7 ¹Center for Atmospheric and Oceanic Studies, Graduate School of Science, Tohoku University, Sendai, Japan

8 ²Center for Environmental Remote Sensing, Chiba University, Chiba, Japan

9 ³Institute of Remote Sensing and Digital Earth, Chinese Academy of Sciences, Beijing, China

10 ⁴Research and Information Center (TRIC), Tokai University, Hiratsuka, Japan

11 ⁵Meteorological Research Institute, Tsukuba, Japan

12

13 *Correspondence to:* Pradeep Khatri (pradeep.khatri.a3@tohoku.ac.jp)

14

15 **Abstract.** The Second-generation Global Imager (SGLI) onboard the Global Change Observation Mission –
16 Climate (GCOM-C) satellite launched on December 23, 2017, observes various geophysical parameters with the
17 aim of a better understanding of the global climate system. As part of that aim, SGLI has great potential to unravel
18 several uncertainties related to clouds by providing new cloud products along with several other atmospheric
19 products related to cloud climatology, including aerosol products from polarization channels. However, a very
20 little is known about the quality of the SGLI cloud products. This study uses data about clouds and global
21 irradiances observed from the Earth’s surface using a sky radiometer and a pyranometer, respectively, to
22 understand the quality of the two most fundamental cloud properties—cloud optical depth (COD) and cloud-
23 particle effective radius (CER)—of both water and ice clouds. The SGLI-observed COD agrees well with values
24 observed from the surface, although it agrees better for water clouds than for ice clouds, while the SGLI-observed
25 CER exhibits poorer agreement than does the COD, with the SGLI values being generally higher than the sky
26 radiometer values. These comparisons between the SGLI and sky radiometer cloud properties are found to differ
27 for different cloud types of both the water and ice cloud phases and different solar and satellite viewing angles by
28 agreeing better for relatively uniform and flat cloud type and for relatively low solar zenith angle. Analyses of
29 SGLI-observed reflectance functions and values calculated by assuming plane-parallel cloud layers suggest that
30 SGLI-retrieved cloud properties can have biases on the solar and satellite viewing angles, similar to other satellite
31 sensors including the Moderate Resolution Imaging Spectroradiometer (MODIS). Furthermore, it is found that the
32 SGLI-observed cloud properties reproduce global irradiances quite satisfactorily for both water and ice clouds by
33 resembling several important features of the COD comparison, such as the better agreement for water clouds than



34 for ice clouds and the tendency to underestimate (resp. overestimate) the COD in SGLI observations for optically
35 thick (resp. thin) clouds.

36

37 **1. Introduction**

38 Clouds play important roles in changing the Earth's climate system (Ramanathan et al., 1989), with profound
39 impacts on the atmospheric heat budget and the hydrological cycle (Rosenfeld et al., 2014). However, their strong
40 spatial and temporal variations as well as their complex interactions with aerosols and meteorology (e.g., Rosenfeld
41 et al., 2014; Khatri et al., 2020) have made it difficult to date to represent clouds accurately in global climate
42 models (Forster et al., 2021). Consequently, the roles of clouds in climate change are very poorly understood, and
43 they are highlighted as important sources of uncertainty in future climate projections (IPCC, 2021). Given their
44 importance, clouds are now being studied from different perspectives and using different methods, one of which
45 is cloud remote sensing from space, which has been in practice since the first successful capture of a cloud picture
46 by a Television InfraRed Observational Satellite (TIROS) launched on April 1, 1960. Since then, cloud remote-
47 sensing technology has advanced greatly, and there are currently several active and passive sensors onboard
48 various polar-orbiting or geostationary satellites to observe clouds from space. Because of their benefits of wide
49 spatial coverage and continuous observations at specific time intervals, satellite cloud products have been used
50 broadly either independently (e.g., Khatri et al., 2021) or combined with technologies such as numerical simulation
51 or artificial intelligence (e.g., Masunaga et al., 2008; Letu et al., 2020, 2021), for a better understanding of cloud
52 climatology as well as energy and water budgets. However, because the same satellite sensor monitors either the
53 whole Earth or a large part of it for a long time and the cloud products are generally generated by processing
54 satellite-received signals using certain physical models and assumptions (e.g., daytime cloud optical depth (COD)
55 and cloud-particle effective radius (CER) are obtained using the reflectance observed at two different wavelengths
56 by assuming clouds to be plane-parallel horizontal (PPH) layers), assessing the quality of such cloud products is a
57 fundamental requirement for using them in scientific research, policy making, and other application areas.
58 Furthermore, such quality-assessment studies help in gathering important information that is useful for developing
59 next-generation satellite sensors and observation techniques that overcome the shortcomings of existing
60 technologies.

61 The Global Change Observation Mission – Climate (GCOM-C) satellite (or “Shikisai” in Japanese) is a polar-
62 orbiting satellite that was launched on December 23, 2017. Onboard is the Second-generation Global Imager
63 (SGLI), which has 16 channels covering the spectrum from ultraviolet to thermal infrared. Of these 16 channels,
64 the 1.05-, 1.63-, and 2.21- μm channels in the shortwave infrared region and the 10.8- μm channel in the thermal
65 region are used to infer the properties of both water and ice clouds (Nakajima et al., 2019). Having entered
66 operation relatively recently, very little is known about the quality of the cloud products generated from the SGLI
67 satellite sensor, thereby emphasizing the need and urgency for assessing the quality of SGLI cloud products. In
68 addition, SGLI is a powerful sensor for observing aerosols because of the inclusion of polarization and
69 bidirectional channels, thereby making it very useful for studying aerosol–cloud interaction with qualitative



70 aerosol data. Therefore, studies related to assessing the quality of SGLI cloud products can also contribute to
71 aerosol–cloud interaction studies performed using SGLI data.

72 A literature review shows the scarcity of quality-assessment studies for SGLI cloud products. Nakajima et al.
73 (2019) performed such a study by comparing SGLI cloud products with those obtained from the Moderate
74 Resolution Imaging Spectroradiometer (MODIS) sensor onboard the Terra satellite; they found very good
75 agreement between the MODIS and SGLI cloud products for both water and ice clouds over both ocean and land
76 surfaces. Because cloud retrievals from MODIS and SGLI are based on the same retrieval framework of Nakajima
77 and King (1990) and similar types of cloud reflectance data, it is very important to assess the quality of SGLI cloud
78 products by using data of different natures obtained from different observation techniques, such as those obtained
79 from surface observations. Damiani et al. (2019) compared SGLI-observed COD with surface-observed values
80 obtained using different instruments, including a sky radiometer and a pyranometer; they found reasonably good
81 agreement between the SGLI and surface observations, but their study was limited to an observation period of a
82 few days (16 days) with very few samples for comparison and for water cloud COD only. By contrast, the present
83 study is designed to use long-term observation data from multiple sites to assess the quality of the properties of
84 both water and ice clouds.

85 This paper is organized as follows. Sections 2 and 3 describe the data and the study method, respectively.
86 Section 4 presents and discusses the results. Finally, section 5 summarizes the main findings of this study.

87

88 **2. Data**

89 **2.1. SKYNET**

90 Data from SKYNET sites in Japan (Table 1) for 2018–2020 were used in the present study. These sites have
91 different atmospheric backgrounds: Chiba and Sendai are urban sites, whereas Hedo-misaki, Fukue-jima, and
92 Miyako-jima are located on the coast of the east China Sea, where a different air mass—either marine or long-
93 range transported continental—prevails in different seasons (Khatri et al., 2010, 2014a), making them unique for
94 studying aerosols and clouds. Except for Sendai, all these sites are “super sites” of SKYNET, being equipped with
95 various instruments for observing aerosols, clouds, radiation, and meteorology. We used two types of SKYNET
96 data as described below.

97

98 **2.1.1. Sky radiometer**

99 Nakajima et al. (2020) described in detail the sky radiometer technology of SKYNET. Although sky radiometer
100 data have been used widely to study aerosol properties (e.g., Hashimoto et al., 2012; Wang et al., 2014; Khatri
101 et al., 2016; Mok et al., 2018; Irie et al., 2019), retrievals of ozone (Khatri et al., 2014b), water vapor (Campanelli
102 et al., 2014), and clouds (Khatri et al., 2019) are also possible from sky radiometer observations. The present study
103 used cloud properties retrieved from a sky radiometer (POM-02; PREDE Co., Ltd., Japan) that observed spectral
104 zenith radiances at 10-min intervals. Of 11 wavelengths between ultraviolet and near-infrared, the zenith radiances
105 observed at 0.87, 1.02, and 1.627 μm were used to obtain COD and CER via a cloud retrieval algorithm by Khatri
106 et al. (2019). Aerosol observations made at the wavelengths of 0.38, 0.4, 0.5, 0.675, 0.87, and 1.02 μm under clear



107 sky conditions were used to derive the temporal (monthly) variations of the calibration constants for the
108 wavelengths of 1.627 μm (absorbing) and 0.87 μm and 1.02 μm (non-absorbing) to convert the observed signals
109 into transmittances. These spectral transmittances were then combined with spectral surface reflectance and
110 precipitable water content (PWC) to retrieve COD and CER simultaneously via an optimal method (Rodgers,
111 2000). The surface reflectance and PWC data were obtained from MODIS and Modern-Era Retrospective Analysis
112 for Research and Applications, Version 2 (MERRA-2), respectively. In retrieving the properties of water clouds,
113 single-scattering properties generated for spherical water cloud droplets estimated from Mie calculations were
114 used, whereas such databases corresponding to the Voronoi model of irregular shapes for ice particles (Ishimoto
115 et al., 2012) were used in retrieving the properties of ice clouds.

116

117 2.1.2. Pyranometer

118 Each SKYNET site in Japan is equipped with a pyranometer (Kipp and Zonen, Holland) to measure
119 downwelling global irradiances. Because the global irradiance over Miyako-jima was observed for only a limited
120 study period, the data from the remaining four sites were used in this study. The observed global irradiances were
121 for the spectral range of 0.315–2.8 μm and for a temporal resolutions of 60 s for Sendai and 20 s for the other sites.

122

123 2.2. SGLI

124 We used the Level 2.0 (Version 2.0) cloud products of SGLI (Nakajima et al., 2019). The GCOM-C satellite
125 carrying the SGLI sensor is timed to cross the equator from north to south at approximately 10:30 AM local time,
126 and the spatial resolution of the SGLI cloud product is 1 km \times 1 km at nadir. The SGLI cloud products were
127 retrieved using the CAPCOM cloud property retrieval algorithm (Nakajima and Nakajima, 1995; Kawamoto et al.,
128 2001; Nakajima et al., 2019), in which the 1.05- and 2.21- μm channels were used as the non-absorbing and
129 absorbing wavelengths, respectively, while developing the look-up table (LUT) of cloud reflectance (Nakajima
130 and King, 1990). The LUTs for water clouds and ice clouds were developed using the single-scattering properties
131 of spherical water cloud droplets calculated using Mie theory and non-spherical Voronoi particles (Ishimoto et al.,
132 2012). Along with those reflectance data, the algorithm also used ancillary data such as vertical profiles of
133 temperature, water vapor, and surface reflectance while retrieving cloud properties (Nakajima et al., 2019).

134

135 3. Study method

136 Depending on the departure of the viewing angle of the satellite sensor from nadir, a parallax—that is, a shift
137 in cloud position (longitude and latitude) from that corresponding to the surface—can occur, and correcting this
138 parallax is important when comparing oblique-view satellite products with observations made either at nadir view
139 from space (e.g., Khatri et al., 2018a) or at zenith view from the surface (e.g., Khatri et al., 2018b). Therefore, the
140 SGLI cloud products were parallax-corrected by using information about cloud-top height, the zenith and azimuth
141 angles of the satellite, and the position (latitude and longitude) of the observation site. Then, if all satellite pixels
142 with 5 \times 5 coverage and the observation site at the central pixel were cloudy, they were used to calculate the
143 average values of COD and CER. They were then compared with the sky radiometer values observed at the surface



144 within ± 30 min of the SGLI observation time. Such averaging practices can address cloud movement (Cess et al.,
145 1996) and are common in validating satellite cloud products using surface observation data. For example, Dong
146 et al. (2008) and Yan et al. (2015) compared CERES-MODIS cloud properties averaged over a $30 \text{ km} \times 30 \text{ km}$
147 square and a circle of 20-km radius around the observation site, respectively, with surface observation values
148 averaged over a 1-h period.

149 The pyranometer-observed global irradiances were further used to assess the quality of the SGLI cloud products.
150 For this purpose, the SGLI cloud properties and ancillary data such as PWC from MERRA-2 and spectral surface
151 reflectance from MODIS were used in an RSTAR radiative-transfer model (Nakajima and Tanaka, 1986, 1988) to
152 calculate downwelling global irradiances in the $0.315\text{--}2.8\text{-}\mu\text{m}$ spectral range. The single-scattering properties
153 obtained from Mie calculations for water clouds and those corresponding to the Voronoi model for ice clouds were
154 used for water and ice clouds, respectively. The modeled global irradiances of the 5×5 pixels centered on the
155 observation site were then averaged to compare with the values observed at the surface for ± 5 min centered on the
156 SGLI observation time.

157 To quantify the degree of agreement between the SGLI and surface observations, the mean bias error (MBE),
158 root-mean-square error (RMSE), and correlation coefficient (r) values were calculated as

$$159 \quad MBE = \frac{1}{n} \sum_{i=1}^n (G_i - S_i), \quad (1)$$

$$160 \quad RMSE = \sqrt{\sum_{i=1}^n \frac{(G_i - S_i)^2}{n}}, \quad (2)$$

$$161 \quad r = \frac{n(\sum_{i=1}^n G_i S_i) - \sum_{i=1}^n G_i \sum_{i=1}^n S_i}{\sqrt{[n \sum_{i=1}^n G_i^2 - (\sum_{i=1}^n G_i)^2][n \sum_{i=1}^n S_i^2 - (\sum_{i=1}^n S_i)^2]}}, \quad (3)$$

162 where G_i and S_i are surface and satellite observations, respectively, and n is the total sample count.

163

164 4. Results and discussion

165 4.1. Comparison between SGLI-observed and sky radiometer-observed cloud properties

166 4.1.1. Overall comparison

167 The COD values from the sky radiometer and SGLI are compared in Figure 1(a) and (b) for water clouds and
168 ice clouds, respectively. In general, the values from the two different sources agree reasonably well for both cloud
169 types. The r value for water clouds is higher than that for ice clouds, suggesting that the temporal variations of
170 COD from the sky radiometer and SGLI are more consistent with each other for water clouds than for ice clouds.
171 The MBE values are positive and nearly the same for water and ice clouds. Overall, these positive MBE values
172 suggest smaller COD from SGLI than from the sky radiometer for both water and ice clouds, but upon closer
173 inspection, Figure 1 indicates that whether the COD from SGLI is an overestimate or an underestimate depends
174 on the COD value; we have underestimated values from SGLI for relatively high COD for both water and ice
175 clouds, whereas most of the data samples show an overestimated COD from SGLI when they are less than ~ 20
176 and ~ 10 for water and ice clouds, respectively. A literature review also suggests similar results in the past for COD
177 observed by other remote-sensing tools. For example, King et al. (2013) and Liu et al. (2013) showed
178 overestimated (resp. underestimated) COD for values less (resp. greater) than ~ 20 when they compared MODIS



179 COD with values obtained from in situ aircraft observations and a multifilter rotating shadowband radiometer,
180 respectively. Nakajima et al. (1991) also found overestimation (resp. underestimation) of COD for values less
181 (resp. greater) than ~ 10 while comparing their products retrieved from cloud reflection measurements with those
182 obtained from in situ aircraft observations. Khatri et al. (2018b) also found similar results when they compared
183 COD values observed by MODIS and the Advanced Himawari Imager with surface-observed values. The
184 consistency of Figure 1 with those previous studies indicates that reflectance-based COD from satellite retrieved
185 by assuming PPH cloud layers (i.e., by using one-dimensional (1D) radiative transfer theory) can be
186 underestimated (resp. overestimated) for optically thin (resp. thick) clouds irrespective of sensor type.

187 The CER values from the sky radiometer and SGLI are compared in Figure 2 (a) and (b) for water clouds and
188 ice clouds, respectively. The CER values show poorer agreement than do the COD values in the comparisons for
189 both water and ice clouds. However, note that CER depends on not only the reflectance function of the absorbing
190 wavelength but also the COD (Zhang and Platnick, 2011). Thus, such poor CER agreement can be due in part to
191 the COD differences between the sky radiometer and SGLI. Additionally, the satellite-observed CER is highly
192 sensitive to the upper cloud layers near the cloud top, whereas the surface-observed CER includes the overall
193 effects of all the cloud layers to result in such poorer agreement in the CER comparisons. Most of the data samples
194 show higher CER values from SGLI than from the sky radiometer, resulting in negative values of MBE for both
195 water and ice clouds. This result is in line with previous studies that showed higher values from satellite
196 observations compared with values obtained from surface and/or aircraft observations (e.g., Painemal and Zuidema,
197 2011; Chiu et al., 2012; King et al., 2013). Despite the poorer agreement for CER, most of the data samples can
198 be seen to fall around the 1:1 line in Figure 2(a) for water clouds. This suggests that the few outliers had a large
199 detrimental effect on the CER comparison for water clouds, indicating that the sky radiometer and SGLI could
200 agree better for not only COD but also CER under certain condition, which will be discussed in the coming sections.

201

202 **4.1.2. Comparison by separate cloud type**

203 The SGLI cloud product also contains information about cloud type, which is determined based on COD and
204 cloud top pressure (CTP), similar to the cloud classification method of the International Satellite Cloud
205 Climatology Project. The data for water clouds shown in Figures 1(a) and 2(a) correspond to the altostratus,
206 nimbostratus, stratocumulus, and stratus cloud types. Figure 3 compares the sky radiometer and SGLI cloud
207 properties for each cloud type. Of these four types of clouds, the first two are mid-level clouds and the last two are
208 low-level clouds, which have CTP value of 440–680 hPa and greater than 680 hPa, respectively. Similarly,
209 altostratus and stratocumulus have COD values of 3.6–23, but nimbostratus and stratus have COD values greater
210 than 23. In Figure 3, stratus clouds show the best agreement; compared to the other types of clouds, stratus clouds
211 are more uniform and flatter, thereby being the closest to PPH cloud layers. After stratus clouds, nimbostratus
212 clouds suggest the next-best agreement, although some CER values show large deviations from the 1:1 line.
213 Because nimbostratus is a thick mid-level cloud, ice crystals or their combination with liquid cloud droplets—
214 including supercooled droplets—can form in and around the cloud top, although middle and lower cloud portions
215 can contain water cloud droplets. Under such conditions, retrievals from SGLI by considering the cloud phase as



216 being water can affect the retrieved products significantly, especially CER, which in turn can cause considerably
217 large differences from the CER observed from the surface. To some extent, the results from the sky radiometer
218 can also be affected, but because it observes from the surface, the larger fractions of water in the middle and lower
219 cloud portions may make considering the water cloud phase reasonably valid for surface observations. On the
220 other hand, altostratus and stratocumulus clouds show moderate agreement for COD but poor agreement for CER.
221 Because these clouds can have COD values ranging from 3.6 to 23, large differences in CER comparison can arise,
222 especially for relatively thin clouds. This is because the uncertainties in CER retrievals can be larger for thin clouds
223 than for thick clouds in both sky radiometer and SGLI retrievals. Additionally, the high-level altostratus cloud can
224 comprise ice and/or supercooled droplets near the cloud top to affect SGLI retrievals, as discussed above.
225 Regarding low-level stratocumulus clouds, they may not contain such ice and/or supercooled liquid particles, but
226 their cloud tops can be quite inhomogeneous because they are generally clumps of thick and thin clouds, resulting
227 in a higher degree of cloud heterogeneity, which in turn can have large effects on satellite retrievals, as revealed
228 from both modeling (e.g., Iwabuchi and Hayasaka, 2002) and observation (e.g., Várnai and Marshak, 2007).
229 Because SGLI has a larger field of view (FOV) than does the sky radiometer, instrumental FOV could be the next
230 important factor for the large difference between the sky radiometer and SGLI results for such highly heterogeneous
231 stratocumulus clouds.

232 Figure 4 compares the sky radiometer-observed and SGLI-observed cloud properties for different types of ice
233 clouds. As shown, seven types of ice phase clouds were detected, of which cirrus, cirrostratus, and deep convective
234 are high-level clouds, altocumulus, altostratus, and nimbostratus are mid-level clouds, and stratocumulus is a low-
235 level cloud. Cirrus and altostratus clouds have COD values of less than 3.6. These thin clouds have values of both
236 COD and CER that deviate largely from the 1:1 line, suggesting that large differences between the sky radiometer
237 and SGLI results can occur for thin clouds. This is because retrievals become ambiguous, resulting in two possible
238 solutions in both satellite retrieval (Nakajima and King, 1990) and sky radiometer retrieval (Khatri et al., 2019)
239 for such thin clouds. Furthermore, the sky radiometer-observed values are averages of ± 30 min centered on the
240 SGLI overpass time, making it possible to include some nearby thick clouds not included in the 5×5 pixels of
241 SGLI observation, given that the wind speed can be high at high altitudes. Cirrostratus followed by altostratus
242 occupy significant numbers of the ice cloud data. Furthermore, these cloud types agree better than do the other
243 types; they are generally uniform stratiform (layered) genus-type, that is, closer to PPH cloud layers than are the
244 other types of clouds. However, despite having the best agreement, some considerably large differences between
245 the sky radiometer and SGLI results still exist; these could be due to high wind speed, especially for cirrostratus,
246 a mixture of both water and ice cloud droplets, especially for altostratus, and the irregular shapes of ice crystals.
247 Deep convective and nimbostratus clouds have COD values of greater than 23. Although the top layers of these
248 clouds generally contain irregularly shaped ice crystals, their middle and lower parts can contain water cloud
249 droplets and/or supercooled droplets, making it difficult to retrieve cloud properties from both SGLI and the sky
250 radiometer by using a database of a single type of cloud phase. These thick clouds suggest fairly good agreement
251 between the sky radiometer and SGLI cloud properties, as do the low-level stratocumulus clouds detected as ice
252 clouds by SGLI.



253 Overall, the above comparison results for different types of clouds for both water and ice phases reveal that
254 cloud properties retrieved from the sky radiometer and SGLI can agree better if the clouds are relatively uniform,
255 flat, and thick.

256

257 **4.1.3. Effects of solar and satellite viewing geometries on comparison results**

258 Satellite cloud products retrieved by assuming PPH cloud layers can have biases depending on solar zenith
259 angle (SZA) (Kato and Marshak, 2009) and satellite viewing zenith angle (VZA) (Várnai and Marshak, 2007). To
260 understand how such SZA and VZA biases might influence the differences between SGLI and sky radiometer
261 cloud properties, comparisons are performed by separating the data for each SZA and VZA greater than and less
262 than 30° . The comparison results corresponding to water and ice clouds are shown in Figures 5 and 6, respectively.
263 To understand further how SZA and VZA biases might influence the comparison results, we calculated the mean
264 values of SZA and VZA for different levels of agreement in the sky radiometer and SGLI comparisons. In other
265 words, these mean values were calculated by identifying very good agreement (difference less than 30%), moderate
266 agreement (difference within 30%–60%), poor agreement (difference within 60%–90%), and very poor agreement
267 (difference greater than 90%), where the difference is $|x_{SGLI} - x_{sky}|/x_{sky} \times 100\%$ and x represents COD or CER.
268 The mean values are summarized in Tables 2 and 3 for water and ice clouds, respectively. Figures 5 and 6 both
269 show better agreements between the sky radiometer and SGLI COD values for $SZA < 30^\circ$ than for $SZA > 30^\circ$.
270 Also, Table 2 suggests that increasing SZA increases the COD difference for water clouds. Although not distinct
271 as in the case of water clouds, the COD difference for ice clouds also indicates its dependency on SZA in Table 3.
272 These results suggest possible SZA bias in SGLI-observed COD and so its influence on the COD differences
273 between the sky radiometer and SGLI. Both observations (e.g., Loeb and Davies, 1997) and radiative-transfer
274 model simulations (e.g., Kato et al., 2006) suggest that COD retrieved by assuming PPH cloud layers increases
275 with SZA because the horizontal leakage of radiation from cloud sides decreases relative to overhead Sun (Fu
276 et al., 2000) and cloud sides have a greater opportunity to intercept more solar radiation for oblique Sun to increase
277 the cloud-top-leaving radiance (Loeb et al., 1997). On the other hand, there appears to be no clear improvement in
278 COD comparison between the sky radiometer and SGLI with increasing or decreasing VZA. However, as revealed
279 from Figure 5, the COD comparison between the sky radiometer and SGLI for water clouds may deteriorate
280 considerably when both SZA and VZA become large. Supporting this result, Table 2 shows higher values of VZA
281 for cases of moderate and poor agreement than for very good and moderate agreement for water clouds. However,
282 there seems to be no clear signature of the dependence of COD difference on VZA for ice clouds in Table 3. Liang
283 and Di Girolamo (2013) suggested that satellite COD retrieved under the assumption of PPH cloud layers can
284 either decrease or increase with VZA depending on the competition among multiple factors governed by SZA,
285 relative azimuth angle (RAZ), and cloud inhomogeneity. This can plausibly explain the unclear effects of VZA on
286 the COD comparisons shown in Figures 5 and 6 and summarized in Tables 2 and 3. For CER, it is almost
287 impossible to say how SZA and VZA influence the CER comparisons shown in Figures 5 and 6, although to some
288 extent it is likely that water clouds exhibit better agreement for low SZA than for high SZA. Coinciding with the
289 results shown in Figures 5 and 6, Tables 2 and 3 also discard the influences of SZA and VZA on the CER



290 differences between the sky radiometer and SGLI. Because the cloud properties observed from SGLI and the sky
291 radiometer depend strongly on cloud type, as discussed above, and CER retrievals have larger uncertainties than
292 do COD retrievals, these factors possibly diluted the influences of SZA and VZA on the CER differences between
293 the sky radiometer and SGLI.

294 SZA and VZA biases on retrieved cloud properties for other satellite sensors—including MODIS—have been
295 studied widely, but such studies for the SGLI sensor have been lacking to date. We further analyzed the SGLI
296 observed reflectance (R) to shed further light on possible biases on the SGLI-retrieved cloud properties. For this
297 purpose, the SGLI-observed R ($1.05\ \mu\text{m}$) data with values of less than 1 for 500 pixels centered on the Chiba
298 observation site were analyzed. Those data correspond to 2020. R values corresponding to different values of COD
299 ($\text{COD} = 2\pm 1, 4\pm 1, 8\pm 1, 16\pm 1, 32\pm 1, 64\pm 1$) and SZA ($\text{SZA} = 20^\circ\pm 1^\circ\text{--}60^\circ\pm 1^\circ$ in 5° intervals) were binned by
300 accounting for the relative azimuth angle (RAZ), that is, the difference in azimuth angles between Sun and satellite.
301 Figure 7 shows the R -VZA relationships for these values of COD and SZA. Negative (resp. positive) VZA
302 corresponds to RAZ greater (resp. less) than 90° , representing forward (resp. backward) scattering. Because the
303 R -VZA relationship is similar for ice clouds, it is not shown here. The data fluctuations in Figure 7 for the same
304 values of COD and SZA suggest variations of CER and surface and atmospheric conditions. To tally such observed
305 R -VZA relationships, we again calculated R ($1.05\ \mu\text{m}$) for the COD values of 2, 4, 8, 16, 32, and 64 with a fixed
306 CER of $8\ \mu\text{m}$ and SZA values of $20^\circ\text{--}60^\circ$ with intervals of 5° by assuming PPH cloud layers (Figure 8). These
307 calculations were performed for RAZ values of 135° and 45° to understand the characteristics of forward and
308 backward scattering, respectively. The calculated results shown in Figure 8 reveal that the R -VZA relationship for
309 ideal PPH cloud layers can have different shapes depending on SZA. For low SZA, the differences in R between
310 the forward and backward scattering directions are relatively small, increasing gradually with increasing SZA; for
311 high values of SZA, the R values in the forward scattering directions are higher than those in the backward
312 scattering direction. The shapes of the R -VZA relationship for ideal PPH cloud layers, which correspond to the
313 LUT databases of satellite retrieval algorithms, are different than those shown in Figure 7 corresponding to actual
314 observations, suggesting that three-dimensional (3D) cloud effects on observed signals are not captured well in
315 1D radiative-transfer calculations. Liang and Girolamo (2013) suggested that the observed VZA dependence of
316 COD (or R) is the weighted sum of different competing factors associated with Sun and satellite positions and
317 cloud inhomogeneity. For example, Várnai and Marsak (2007) found increased values of COD with increasing
318 VZA in both the forward and backward scattering directions, and they suggested that the dark gaps between cloud
319 fields could be filled up by brighter cloud sides through photon leakage when partly cloudy scenes are viewed
320 more obliquely, leading to higher values of COD in both the forward and backward scattering directions. On the
321 other hand, Loeb and Coakley (1998) found decreased and increased COD in the forward and backward scattering
322 directions, respectively, which they attributed to shadowing and illumination. Nevertheless, the most important
323 information revealed from Figures 7 and 8 is that 1D radiative-transfer theory may hardly capture the features of
324 R observed by SGLI, suggesting SZA and VZA biases on the retrieved cloud properties from SGLI, similar to
325 other satellite sensors including MODIS.

326



327 **4.2. Comparison between modeled and observed global irradiances**

328 Because surface-observed global irradiances vary strongly with cloud variation (Khatri and Takamura, 2009;
329 Damiani et al., 2018), they can also help to justify the comparison results discussed above. Specifically, surface-
330 observed global irradiances can be effective for evaluating satellite-observed COD values because the variation of
331 COD is more dominant than the variation of CER in the variation of global irradiance (Khatri et al., 2018b).
332 Figure 9 compares the measured and modeled global irradiances at the four observation sites that have observation
333 data for the whole study period for water clouds (Figure 9(a)) and ice clouds (Figure 9(b)). These comparisons are
334 for the mean values of the 5×5 SGLI pixels and ± 5 min of surface observations centered on the SGLI observation
335 time. The measured global irradiances agree very well with the observed values for both water clouds and ice
336 clouds. In both cases, the correlations are very strong with values greater than 0.85. The RMSE value for water
337 clouds is smaller than that for ice clouds, suggesting that water cloud optical properties can reproduce global
338 irradiance better than can ice cloud properties. Although not distinctly different, the absolute MBE value is smaller
339 for water clouds than for ice clouds. Overall, these results suggest that retrieval accuracies are better for water
340 cloud properties than for ice cloud properties in SGLI. Note that the COD values from the sky radiometer also
341 agree better for water clouds than for ice clouds. The MBE values are negative for both water and ice clouds,
342 suggesting that the modeled global irradiances are generally higher than the observed values. Such negative MBE
343 values (overestimation of modeled global irradiances) can result from underestimated COD values in SGLI. This
344 result again coincides with the positive MBE values for the comparisons of COD between the sky radiometer and
345 SGLI shown in Figure 1. Furthermore, Figure 10 shows scatter plots for the normalized differences between the
346 modeled and measured values and the observed values. The observed global irradiance can suggest the COD, with
347 a low global irradiance corresponding to a high COD and vice versa. Figure 10 suggests overestimated values of
348 the modeled global irradiance when the observed values are relatively low, suggesting underestimated COD in
349 SGLI when the clouds are optically thick. This result again coincides with the comparison of COD between the
350 sky radiometer and SGLI shown in Figure 1 and discussed in section 4.1.1. The fewer data samples for water
351 clouds hardly suggest underestimated modeled irradiance (overestimated SGLI COD) when the observed global
352 irradiance is relatively high, but it is somewhat evident in ice clouds. This result again supports the underestimation
353 (resp. overestimation) of COD from SGLI when the clouds are relatively thick (resp. thin), as discussed in section
354 4.1.1.

355 Unlike the COD comparisons shown for different cloud types and SZA and VZA values, the measured and
356 modeled global irradiances do not show distinct differences depending on cloud type and SZA and VZA values.
357 This is likely due to the fact that the global-irradiance-observing pyranometer has a wide FOV. Khatri et al. (2019)
358 discussed the importance of an instrument's FOV for cloud remote sensing.

359

360 **5. Conclusions**

361 The main findings of this study are summarized below.

- 362 1. The COD values from SGLI agreed reasonably well with the values observed from the surface using a sky
363 radiometer by showing correlation coefficient (r) values of ~ 0.8 and ~ 0.6 , RMSE values of ~ 10 and ~ 8 , and



364 MBE values of ~ 3 and ~ 3 for water and ice clouds, respectively. There appears to be a tendency of
365 underestimating (resp. overestimating) the COD in SGLI for relatively thick (resp. thin) clouds. By contrast,
366 the CER comparisons showed poorer agreements than the COD values, with r values of ~ 0.1 and ~ 0.3 , RMSE
367 values of ~ 7 and $\sim 18 \mu\text{m}$, and MBE values of ~ -0.5 and $\sim -10 \mu\text{m}$ for water and ice clouds, respectively.

- 368 2. Comparison analyses performed by separating cloud types revealed that relatively thin, possibly mixed, and
369 horizontally inhomogeneous cloud types generally have larger discrepancies than do relatively uniform and
370 flat types of clouds for both the water and ice phases of clouds.
- 371 3. The COD differences between SGLI and the sky radiometer showed strong and weak dependencies on SZA
372 for water and ice clouds, respectively, by showing increasing difference with increasing SZA. On the other
373 hand, only the COD difference for water clouds showed a weak dependency on VZA, with increased
374 difference for high VZA.
- 375 4. Analyses of the SGLI-observed reflection as functions of SZA, VZA, and COD and similar values of
376 computed reflection functions by using a 1D radiative-transfer model (assuming PPH cloud layers) were
377 inconsistent with each other, indicating that the 1D model was insufficient for capturing 3D cloud effects on
378 the observed signals and thereby SZA and VZA biases on the retrieved cloud properties.
- 379 5. The surface global irradiances calculated using the SGLI-observed cloud properties agreed very well with
380 the surfaced-observed values, with r values of ~ 0.9 and ~ 0.9 , RMSE values of ~ 66 and $\sim 91 \text{ Wm}^{-2}$, and MBE
381 values of ~ -32 and $\sim -33 \text{ Wm}^{-2}$ for water and ice clouds, respectively. These results further revealed higher
382 values of modeled irradiances than observed values when the latter were relatively low, and vice versa. These
383 results further justified the evaluations of SGLI COD performed using the sky radiometer by emphasizing
384 that (i) the SGLI COD can be underestimated on average, (ii) water cloud properties may have better retrieval
385 accuracies than do ice cloud properties, and (iii) the SGLI COD can be underestimated (resp. underestimated)
386 for optically thick (resp. thin) clouds.

387
388 *Code availability.* Codes for data analyses are available from the corresponding author upon request.
389

390 *Data availability.* SGLI data can be downloaded from Global Portal System (G-portal) of JAXA
391 (<https://gportal.jaxa.jp/gpr/>). Similarly, global irradiance data can be downloaded from SKYNET webpage
392 (<http://atmos3.cr.chiba-u.jp/skynet/>). Cloud properties retrieved from sky radiometer observations can be obtained
393 from the corresponding author upon request.

394
395 *Author contributions.* PK and TH developed the study framework. HI and TT generated data. PK, HL, TN, and HI
396 developed algorithms.

397
398 *Competing interests.* The authors declare that they have no conflict of interest.
399



400 *Special issue statement.* This article is part of the special issue “SKYNET – the international network for aerosol,
401 clouds, and so- lar radiation studies and their applications (AMT/ACP inter-journal SI)”. It is not associated with
402 a conference.

403

404 *Acknowledgements:* This research is supported by the 2nd Research Announcement on the Earth Observations of
405 the Japan Aerospace Exploration Agency (JAXA) (PI No. ER2GCF211, Contract No. 19RT000370), a Grant-in-
406 Aid for Scientific Research (C) 17K05650 from Japan Society for the Promotion of Science (JSPS), and “Virtual
407 Laboratory for Diagnosing the Earth’s Climate System” program of MEXT, Japan.

408

409 **References**

410 Campanelli, M., Nakajima, T., Khatri, P., Takamura, T., Uchiyama, A., Estelles, V., Liberti, G. L., and Malvestuto,
411 V.: Retrieval of characteristic parameters for water vapour transmittance in the development of ground-based
412 sun–sky radiometric measurements of columnar water vapour, *Atmospheric Measurement Techniques*, 7,
413 1075-1087, 10.5194/amt-7-1075-2014, 2014.

414 Cess, R. D., Zhang, M. H., Zhou, Y., Jing, X., and Dvortsov, V.: Absorption of solar radiation by clouds:
415 Interpretations of satellite, surface, and aircraft measurements, *Journal of Geophysical Research: Atmospheres*,
416 101, 23299-23309, 10.1029/96jd02156, 1996.

417 Chiu, J. C., Marshak, A., Huang, C. H., Várnai, T., Hogan, R. J., Giles, D. M., Holben, B. N., O’Connor, E. J.,
418 Knyazikhin, Y., and Wiscombe, W. J.: Cloud droplet size and liquid water path retrievals from zenith radiance
419 measurements: examples from the Atmospheric Radiation Measurement Program and the Aerosol Robotic
420 Network, *Atmospheric Chemistry and Physics*, 12, 10313-10329, 10.5194/acp-12-10313-2012, 2012.

421 Damiani, A., Irie, H., Horio, T., Takamura, T., Khatri, P., Takenaka, H., Nagao, T., Nakajima, T. Y., and Cordero,
422 R. R.: Evaluation of Himawari-8 surface downwelling solar radiation by ground-based measurements,
423 *Atmospheric Measurement Techniques*, 11, 2501-2521, 10.5194/amt-11-2501-2018, 2018.

424 Damiani, A., Irie, H., Takamura, T., Kudo, R., Khatri, P., Iwabuchi, H., Masuda, R., and Nagao, T.: An Intensive
425 Campaign-Based Intercomparison of Cloud Optical Depth from Ground and Satellite Instruments under
426 Overcast Conditions, *Sola*, 15, 198-204, 10.2151/sola.2019-036, 2019.

427 Dong, X., Minnis, P., Xi, B., Sun-Mack, S., and Chen, Y.: Comparison of CERES-MODIS stratus cloud properties
428 with ground-based measurements at the DOE ARM Southern Great Plains site, *Journal of Geophysical
429 Research*, 113, 10.1029/2007jd008438, 2008.

430 Forster, P., T. Storelvmo, K. Armour, W. Collins, J.-L. Dufresne, D. Frame, D.J. Lunt, T. Mauritsen, M.D. Palmer,
431 M. Watanabe, M. Wild, and H. Zhang: The Earth’s Energy Budget, Climate Feedbacks, and Climate Sensitivity.
432 In *Climate Change 2021: The Physical Science Basis. Contribution of Working Group I to the Sixth
433 Assessment Report of the Intergovernmental Panel on Climate Change* [Masson-Delmotte, V., P. Zhai, A.
434 Pirani, S.L. Connors, C. Péan, S. Berger, N. Caud, Y. Chen, L. Goldfarb, M.I. Gomis, M. Huang, K. Leitzell,
435 E. Lonnoy, J.B.R. Matthews, T.K. Maycock, T. Waterfield, O. Yelekçi, R. Yu, and B. Zhou (eds.)]. Cambridge
436 University Press. In Press., 2021.



- 437 Fu, Q., Cribb, M. C., Barker, H. W., Krueger, S. K., and Grossman A.: Cloud geometry effects on atmospheric
438 solar absorption, *Journal of the Atmospheric Sciences*, 57, 1156–1168, doi:10.1175/1520-
439 0469(2000)057<1156:CGEOAS>2.0.CO;2, 2000.
- 440 Hashimoto, M., Nakajima, T., Dubovik, O., Campanelli, M., Che, H., Khatri, P., Takamura, T., and Pandithurai,
441 G.: Development of a new data-processing method for SKYNET sky radiometer observations, *Atmospheric*
442 *Measurement Techniques*, 5, 2723–2737, 10.5194/amt-5-2723-2012, 2012.
- 443 IPCC: Climate Change 2021: The Physical Science Basis. Contribution of Working Group I to the Sixth
444 Assessment Report of the Intergovernmental Panel on Climate Change [Masson-Delmotte, V., P. Zhai, A.
445 Pirani, S.L. Connors, C. Péan, S. Berger, N. Caud, Y. Chen, L. Goldfarb, M.I. Gomis, M. Huang, K. Leitzell,
446 E. Lonnoy, J.B.R. Matthews, T.K. Maycock, T. Waterfield, O. Yelekçi, R. Yu, and B. Zhou (eds.)]. Cambridge
447 University Press. In Press., 2021.
- 448 Irie, H., Hoque, H. M. S., Damiani, A., Okamoto, H., Fatmi, A. M., Khatri, P., Takamura, T., and Jarupongsakul,
449 T.: Simultaneous observations by sky radiometer and MAX-DOAS for characterization of biomass burning
450 plumes in central Thailand in January–April 2016, *Atmospheric Measurement Techniques*, 12, 599–606,
451 10.5194/amt-12-599-2019, 2019.
- 452 Ishimoto, H., Masuda, K., Mano, Y., Orikasa, N., and Uchiyama, A.: Irregularly shaped ice aggregates in optical
453 modeling of convectively generated ice clouds, *Journal of Quantitative Spectroscopy and Radiative Transfer*,
454 113, 632–643, 10.1016/j.jqsrt.2012.01.017, 2012.
- 455 Iwabuchi, H., and Tadahiro, H.: Effects of Cloud Horizontal Inhomogeneity on the Optical Thickness Retrieved
456 from Moderate-Resolution Satellite Data, *Journal of the Atmospheric Sciences*, 59, 2227–2242,
457 [https://doi.org/10.1175/1520-0469\(2002\)059<2227:EOCHIO>2.0.CO;2](https://doi.org/10.1175/1520-0469(2002)059<2227:EOCHIO>2.0.CO;2), 2002.
- 458 Kato, S., Hinkelman, L. M., and Cheng, A.: Estimate of satellite-derived cloud optical thickness and effective
459 radius errors and their effect on computed domain-averaged irradiances, *Journal of Geophysical Research*, 111,
460 10.1029/2005jd006668, 2006.
- 461 Kato, S. and Marshak, A.: Solar zenith and viewing geometry-dependent errors in satellite retrieved cloud optical
462 thickness: Marine stratocumulus case, *Journal of Geophysical Research: Atmospheres*, 114,
463 10.1029/2008jd010579, 2009.
- 464 Kawamoto, K., Nakajima, T., and Nakajima, T. Y.: A Global Determination of Cloud Microphysics with AVHRR
465 Remote Sensing, *Journal of Climate*, 14, 4043–4059, [https://doi.org/10.1175/1520-
466 0469\(1995\)052<4043:WADOCM>2.0.CO;2](https://doi.org/10.1175/1520-0469(1995)052<4043:WADOCM>2.0.CO;2), 2000.
- 467 Khatri, P., Hayasaka, T., Holben, B., Tripathi, S. N., Misra, P., Patra, P. K., Hayashida, S., and Dumka, U. C.:
468 Aerosol Loading and Radiation Budget Perturbations in Densely Populated and Highly Polluted Indo-Gangetic
469 Plain by COVID-19: Influences on Cloud Properties and Air Temperature, *Geophysical Research Letters*, 48,
470 10.1029/2021gl093796, 2021.
- 471 Khatri, P., Hayasaka, T., Iwabuchi, H., Takamura, T., Irie, H., and Nakajima, T. Y.: Validation of MODIS and
472 AHI Observed Water Cloud Properties Using Surface Radiation Data, *Journal of the Meteorological Society*
473 of Japan. Ser. II, 96B, 151–172, 10.2151/jmsj.2018-036, 2018b.



- 474 Khatri, P., Iwabuchi, H., Hayasaka, T., Irie, H., Takamura, T., Yamazaki, A., Damiani, A., Letu, H., and Kai, Q.:
475 Retrieval of cloud properties from spectral zenith radiances observed by sky radiometers, *Atmospheric*
476 *Measurement Techniques*, 12, 6037-6047, 10.5194/amt-12-6037-2019, 2019.
- 477 Khatri, P., Iwabuchi, H., and Saito, M.: Vertical Profiles of Ice Cloud Microphysical Properties and Their Impacts
478 on Cloud Retrieval Using Thermal Infrared Measurements, *Journal of Geophysical Research: Atmospheres*,
479 123, 5301-5319, 10.1029/2017jd028165, 2018a.
- 480 Khatri, P., Ooashi, H., and Iwabuchi, H.: Investigating Aerosol Effects on Maritime Deep Convective Clouds
481 Using Satellite and Reanalysis Data, *Sola*, 16, 228-232, 10.2151/sola.2020-038, 2020.
- 482 Khatri, P. and Takamura, T.: An Algorithm to Screen Cloud Affected Data for Sky Radiometer Data Analysis,
483 *Journal of the Meteorological Society of Japan*, 87, 189-204, 10.2151/jmsj.87.189, 2009.
- 484 Khatri, P., Takamura, T., Shimizu, A., and Sugimoto, N.: Spectral Dependency of Aerosol Light-Absorption over
485 the East China Sea Region, *Sola*, 6, 1-4, 10.2151/sola.2010-001, 2010.
- 486 Khatri, P., Takamura, T., Shimizu, A., and Sugimoto, N.: Observation of low single scattering albedo of aerosols
487 in the downwind of the East Asian desert and urban areas during the inflow of dust aerosols, *Journal of*
488 *Geophysical Research: Atmospheres*, 119, 787-802, 10.1002/2013jd019961, 2014a.
- 489 Khatri, P., Takamura, T., Yamazaki, A., and Uchiyama, A.: Use of 315 nm Channel Data of the Sky Radiometer
490 to Estimate the Columnar Ozone Concentration: A Preliminary Study, *Journal of the Meteorological Society*
491 *of Japan. Ser. II*, 92A, 185-194, 10.2151/jmsj.2014-A12, 2014b.
- 492 Khatri, P., Takamura, T., Nakajima, T., Estellés, V., Irie, H., Kuze, H., Campanelli, M., Sinyuk, A., Lee, S. M.,
493 Sohn, B. J., Pandithurai, G., Kim, S. W., Yoon, S. C., Martinez-Lozano, J. A., Hashimoto, M., Devara, P. C.
494 S., and Manago, N.: Factors for inconsistent aerosol single scattering albedo between SKYNET and
495 AERONET, *Journal of Geophysical Research: Atmospheres*, 121, 1859-1877, 10.1002/2015jd023976, 2016.
- 496 King, N. J., Bower, K. N., Crosier, J., and Crawford, I.: Evaluating MODIS cloud retrievals with in situ
497 observations from VOCALS-REx, *Atmospheric Chemistry and Physics*, 13, 191-209, 10.5194/acp-13-191-
498 2013, 2013.
- 499 Letu, H., Nakajima, T. Y., Wang, T., Shang, H., Ma, R., Yang, K., Baran, A. J., Riedi, J., Ishimoto, H., Yoshida,
500 M., Shi, C., Khatri, P., Du, Y., Chen, L., and Shi, J.: A new benchmark for surface radiation products over the
501 East Asia-Pacific region retrieved from the Himawari-8/AHI next-generation geostationary satellite, *Bulletin*
502 *of the American Meteorological Society*, 1-40, 10.1175/bams-d-20-0148.1, 2021.
- 503 Letu, H., Yang, K., Nakajima, T. Y., Ishimoto, H., Nagao, T. M., Riedi, J., Baran, A. J., Ma, R., Wang, T., Shang,
504 H., Khatri, P., Chen, L., Shi, C., and Shi, J.: High-resolution retrieval of cloud microphysical properties and
505 surface solar radiation using Himawari-8/AHI next-generation geostationary satellite, *Remote Sensing of*
506 *Environment*, 239, 10.1016/j.rse.2019.111583, 2020.
- 507 Liang, L. and Girolamo, L. D.: A global analysis on the view-angle dependence of plane-parallel oceanic liquid
508 water cloud optical thickness using data synergy from MISR and MODIS, *Journal of Geophysical Research:*
509 *Atmospheres*, 118, 2389-2403, 10.1029/2012jd018201, 2013.



- 510 Liu, J., Li, Z., Zheng, Y., Chiu, J. C., Zhao, F., Cadeddu, M., Weng, F., and Cribb, M.: Cloud optical and
511 microphysical properties derived from ground-based and satellite sensors over a site in the Yangtze Delta
512 region, *Journal of Geophysical Research: Atmospheres*, 118, 9141–9152, 10.1002/jgrd.50648, 2013.
- 513 Loeb, N. G., and Coakley, Jr., J. A. : Inference of marine stratus cloud optical depths from satellite measurements:
514 Does 1D theory apply?, *Journal of Climate*, 11, 215–233, doi:10.1175/1520-
515 0442(1998)011<0215:IOMSCO>2.0.CO;2, 1998.
- 516 Loeb, N. G., and Davies, R. : Angular dependence of observed reflectances: A comparison with plane parallel
517 theory, *Journal of Geophysical Research: Atmospheres*, 102, 6865–6881, 10.1029/96JD03586, 1997.
- 518 Loeb, N. G., Várnai, T., and Davies, R.: Effect of cloud inhomogeneities on the solar zenith angle dependence of
519 nadir reflectance, *Journal of Geophysical Research: Atmospheres*, 102(DD8), 9387–9395,
520 doi:10.1029/96JD03719, 1997.
- 521 Masunaga, H., Satoh, M., and Miura, H.: A joint satellite and global cloud-resolving model analysis of a Madden-
522 Julian Oscillation event: Model diagnosis, *Journal of Geophysical Research*, 113, 10.1029/2008jd009986, 2008.
- 523 Mok, J., Krotkov, N. A., Torres, O., Jethva, H., Li, Z., Kim, J., Koo, J.-H., Go, S., Irie, H., Labow, G., Eck, T. F.,
524 Holben, B. N., Herman, J., Loughman, R. P., Spinei, E., Lee, S. S., Khatri, P., and Campanelli, M.:
525 Comparisons of spectral aerosol single scattering albedo in Seoul, South Korea, *Atmospheric Measurement*
526 *Techniques*, 11, 2295–2311, 10.5194/amt-11-2295-2018, 2018.
- 527 Nakajima, T., Campanelli, M., Che, H., Estellés, V., Irie, H., Kim, S.-W., Kim, J., Liu, D., Nishizawa, T.,
528 Pandithurai, G., Soni, V. K., Thana, B., Tugjurn, N.-U., Aoki, K., Go, S., Hashimoto, M., Higurashi, A.,
529 Kazadzis, S., Khatri, P., Kouremeti, N., Kudo, R., Marengo, F., Momoi, M., Ningombam, S. S., Ryder, C. L.,
530 Uchiyama, A., and Yamazaki, A.: An overview of and issues with sky radiometer technology and SKYNET,
531 *Atmospheric Measurement Techniques*, 13, 4195–4218, 10.5194/amt-13-4195-2020, 2020.
- 532 Nakajima, T. and King, M. D.: Determination of the Optical Thickness and Effective Particle Radius of Clouds
533 from Reflected Solar Radiation Measurements. Part I: Theory, *Journal of the Atmospheric Sciences*, 47, 1878–
534 1893, [https://doi.org/10.1175/1520-0469\(1990\)047<1878:DOTOTA>2.0.CO;2](https://doi.org/10.1175/1520-0469(1990)047<1878:DOTOTA>2.0.CO;2), 1990.
- 535 Nakajima, T., King, M. D., Spinfire, J. D., and Radke, L. F.: Determination of the Optical Thickness and Effective
536 Particle Radius of Clouds from Reflected Solar Radiation Measurements. Part II: Marine Stratocumulus
537 Observations, *Journal of the Atmospheric Sciences*, 48, 728–751, [https://doi.org/10.1175/1520-
538 0469\(1991\)048<0728:DOTOTA>2.0.CO;2](https://doi.org/10.1175/1520-0469(1991)048<0728:DOTOTA>2.0.CO;2), 1991.
- 539 Nakajima, T., and Tanaka M.: Matrix formulation for the transfer of solar radiation in a plane-parallel scattering
540 atmosphere, *Journal of Quantitative Spectroscopy & Radiative Transfer*, 35, 13–21, 10.1016/0022-
541 4073(86)90088-9, 1986.
- 542 Nakajima, T., and Tanaka M.: Algorithms for radiative intensity calculations in moderately thick atmospheres
543 using a truncation approximation, *Journal of Quantitative Spectroscopy & Radiative Transfer*, 40, 51–69,
544 10.1016/0022-4073(88)90031-3, 1988.



- 545 Nakajima, T. Y., Ishida, H., Nagao, T. M., Hori, M., Letu, H., Higuchi, R., Tamaru, N., Imoto, N., and Yamazaki,
546 A.: Theoretical basis of the algorithms and early phase results of the GCOM-C (Shikisai) SGLI cloud products,
547 Progress in Earth and Planetary Science, 6, 10.1186/s40645-019-0295-9, 2019.
- 548 Nakajima, T. Y. and Nakajima, T.: Wide-Area Determination of Cloud Microphysical Properties from NOAA
549 AVHRR Measurements for FIRE and ASTEX Regions, Journal of Atmospheric Sciences, 52, 4043–4059,
550 [https://doi.org/10.1175/1520-0469\(1995\)052<4043:WADOCM>2.0.CO;2](https://doi.org/10.1175/1520-0469(1995)052<4043:WADOCM>2.0.CO;2), 1995.
- 551 Painemal, D. and Zuidema, P.: Assessment of MODIS cloud effective radius and optical thickness retrievals over
552 the Southeast Pacific with VOCALS-REX in situ measurements, Journal of Geophysical Research:
553 Atmospheres, 116, n/a-n/a, 10.1029/2011jd016155, 2011.
- 554 Ramanathan, V., Cess, R. D., Harrison, E. F., Minnis, P., Barkstrom, B. R., Ahmad, E., and Hartmann, D.: Cloud-
555 radiative forcing and climate: results from the Earth radiation budget experiment, Science, 243, 57-63,
556 10.1126/science.243.4887.57, 1989.
- 557 Rodgers, C. D.: Inverse Methods for Atmospheric Sounding: Theory and Practice (Vol. 2), Ser. Atmos. Oceanic
558 Planet. Phys., 2, World Sci., Hackensack, NJ, 2000.
- 559 Rosenfeld, D., Andreae, M. O., Asmi, A., Chin, M., de Leeuw, G., Donovan, D. P., Kahn, R., Kinne, S., Kivekäs,
560 N., Kulmala, M., Lau, W., Schmidt, K. S., Suni, T., Wagner, T., Wild, M., and Quaas, J.: Global observations
561 of aerosol-cloud-precipitation-climate interactions, Reviews of Geophysics, 52, 750-808,
562 10.1002/2013rg000441, 2014.
- 563 Várnai, T. and Marshak, A.: View angle dependence of cloud optical thicknesses retrieved by Moderate Resolution
564 Imaging Spectroradiometer (MODIS), Journal of Geophysical Research, 112, 10.1029/2005jd006912, 2007.
- 565 Wang, Z., Liu, D., Wang, Z., Wang, Y., Khatri, P., Zhou, J., Takamura, T., and Shi, G.: Seasonal characteristics
566 of aerosol optical properties at the SKYNET Hefei site (31.90°N, 117.17°E) from 2007 to 2013, Journal of
567 Geophysical Research: Atmospheres, 119, 6128-6139, 10.1002/2014jd021500, 2014.
- 568 Yan, H., Huang, J., Minnis, P., Yi, Y., Sun-Mack, S., Wang, T., and Nakajima, T. Y.: Comparison of CERES-
569 MODIS cloud microphysical properties with surface observations over Loess Plateau, Journal of Quantitative
570 Spectroscopy and Radiative Transfer, 153, 65-76, 10.1016/j.jqsrt.2014.09.009, 2015.
- 571 Zhang, Z. and Platnick, S.: An assessment of differences between cloud effective particle radius retrievals for
572 marine water clouds from three MODIS spectral bands, Journal of Geophysical Research, 116,
573 10.1029/2011jd016216, 2011.
- 574
575
576
577
578
579
580
581



582 Table 1. SKYNET sites for surface observation data

Location	Longitude (°E)	Latitude (°N)
Chiba	140.104	35.625
Hedo-misaki	128.248	26.867
Fukue-jima	128.682	32.752
Miyako-jima*	125.327	24.737
Sendai	140.839	38.259

583 *Missing of surface radiative flux data

584

585 Table 2. Mean values of SZA and VZA for different levels of differences in water cloud properties observed by
 586 sky radiometer and SGLI

Diff. Range	COD			CER		
	SZA(°)	VZA(°)	N	SZA(°)	VZA(°)	N
0-30%	35.76±11.42	25.66±15.20	43	37.35±12.59	27.07±14.07	34
30-60%	38.41±8.44	23.68±16.83	13	36.99±10.11	26.90±16.72	20
60-90%	48.52±9.37	29.77±12.53	5	42.70±10.38	25.32±11.26	4
> 90%	53.10±2.84	29.05±5.28	3	43.03±7.16	14.58±12.80	6

587

588

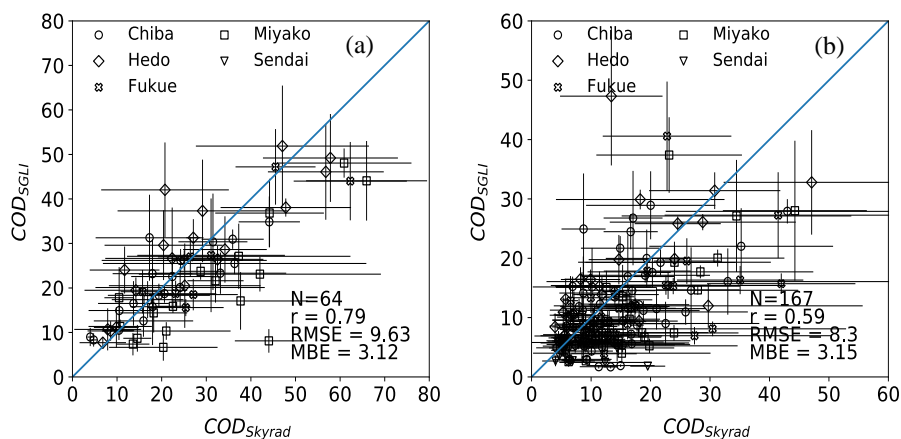
589 Table 3. Mean values of SZA and VZA for different levels of differences in ice cloud properties observed by sky
 590 radiometer and SGLI

Diff. Range	COD			CER		
	SZA(°)	VZA(°)	N	SZA(°)	VZA(°)	N
0-30%	33.62±12.67	26.96±12.67	63	31.29±12.51	25.97±14.27	53
30-60%	32.09±12.65	27.60±14.46	72	33.62±13.27	27.63±12.32	30
60-90%	33.75±12.22	25.89±13.52	29	32.95±13.98	27.31±12.19	25
> 90%	44.20±12.25	26.08±13.96	9	36.62±12.34	27.85±14.02	52

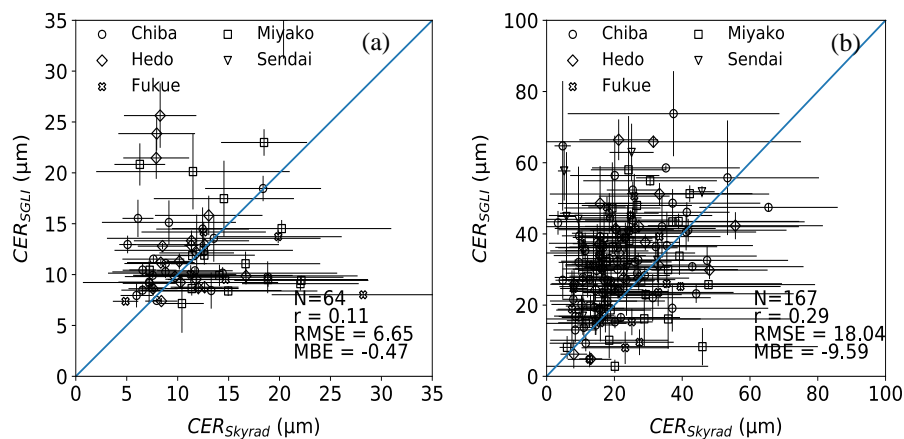
591

592

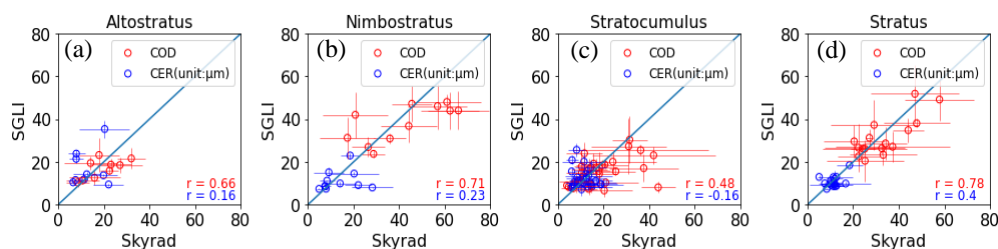
593



594
 595 **Figure 1. Comparison of COD between sky radiometer and SGLI for (a) water clouds and (b) ice clouds**
 596 **for data collected over SKYNET sites.**
 597
 598
 599



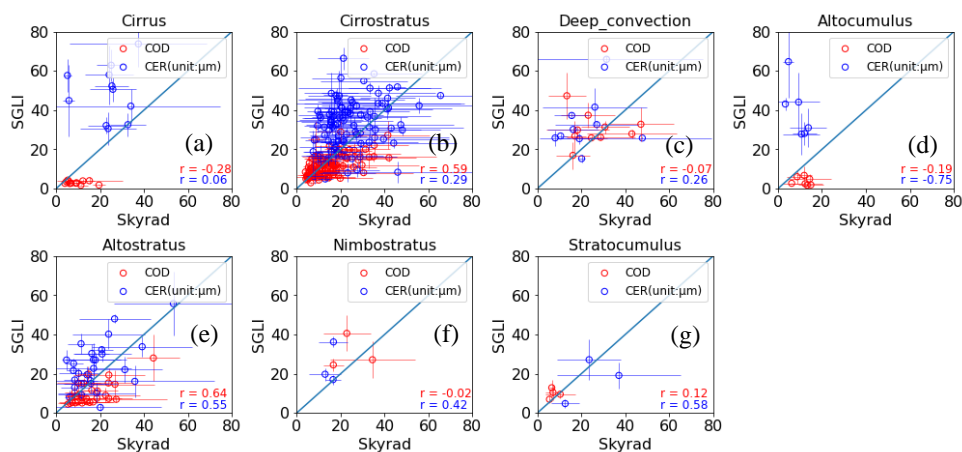
600
 601
 602 **Figure 2. As Figure 1 but for CER.**
 603
 604
 605
 606
 607



608

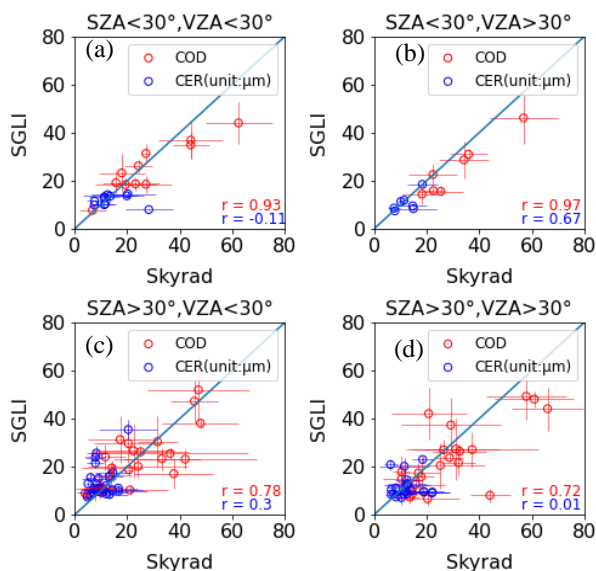
609 **Figure 3. Comparison between sky radiometer-observed and SGLI-observed water cloud properties for**
 610 **different types of clouds.**

611



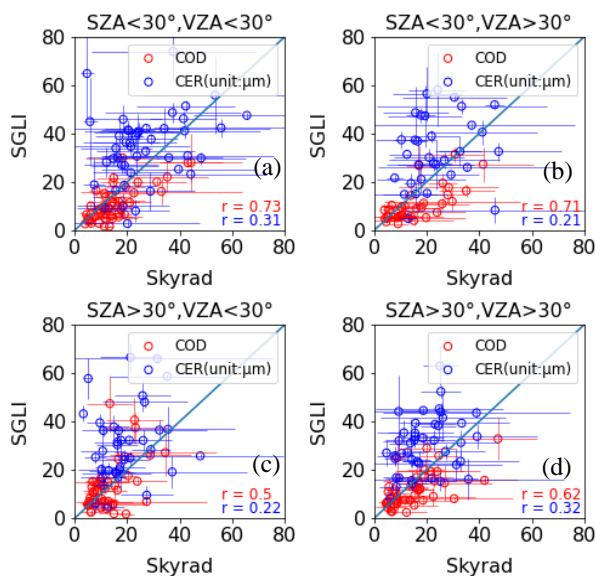
612

613 **Figure 4. As Figure 3 but for ice cloud properties.**



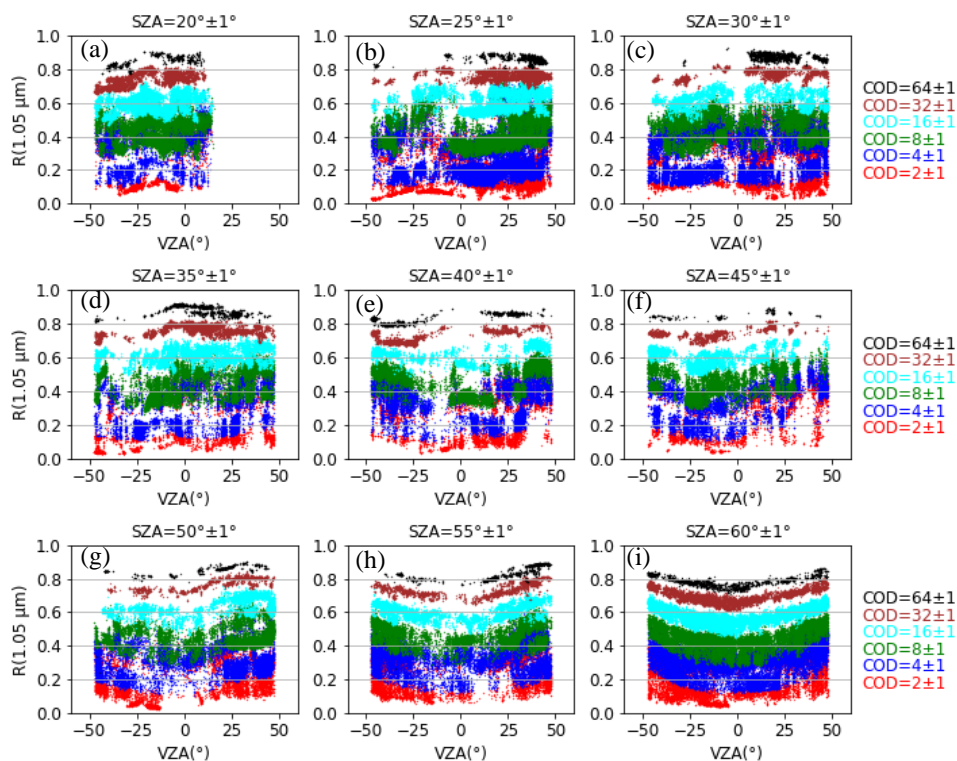
614

615 **Figure 5. Comparison between sky radiometer-observed and SGLI-observed water cloud properties for**
 616 **each SZA and VZA greater than and less than 30°.**



617

618 **Figure 6. As Figure 5 but for ice cloud properties.**



619

620 **Figure 7.** Scatter plots of observed $R(1.05 \mu\text{m})$ – VZA relationships for different COD values of water clouds
621 at different SZA values. The data are for 500 pixels centered on the Chiba observation site in 2020. The
622 negative and positive VZA values represent the forward ($RAZ > 90^\circ$) and backward ($RAZ < 90^\circ$) scattering
623 directions, respectively.

624

625

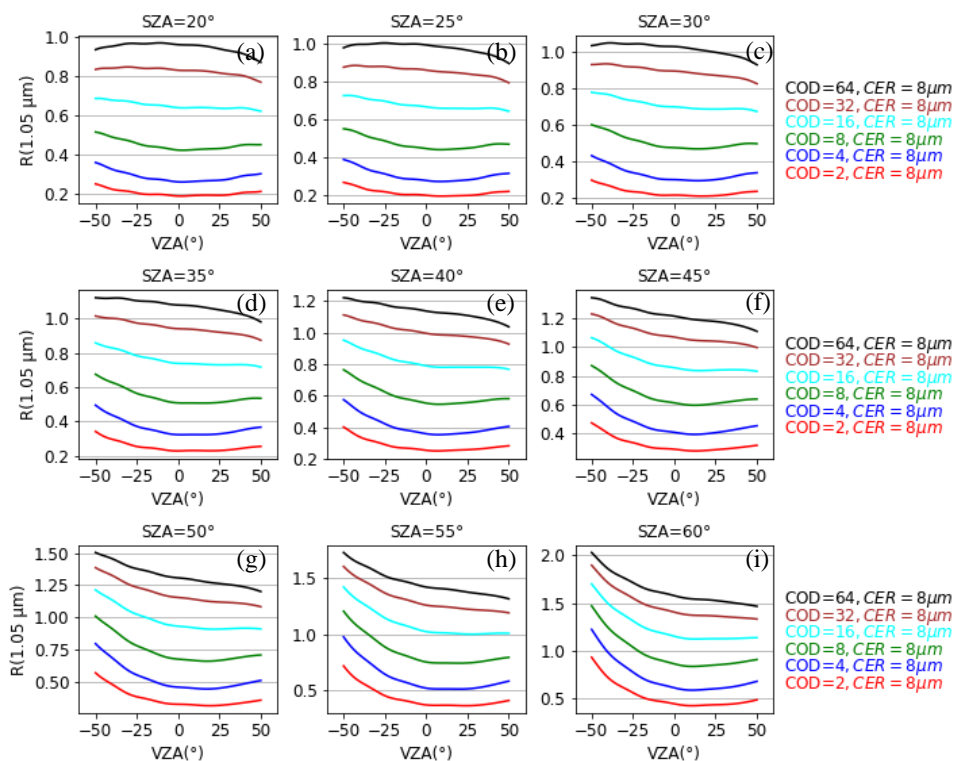
626

627

628

629

630



631

632 **Figure 8. Relationship between $R(1.05 \mu\text{m})$ and VZA for different COD values and fixed CER of $8 \mu\text{m}$ for**
633 **water clouds and different SZA values for assumption of plane-parallel cloud layers. The negative and**
634 **positive VZA values correspond to RAZ values of 135° and 45° representing the forward and backward**
635 **scattering directions, respectively.**

636

637

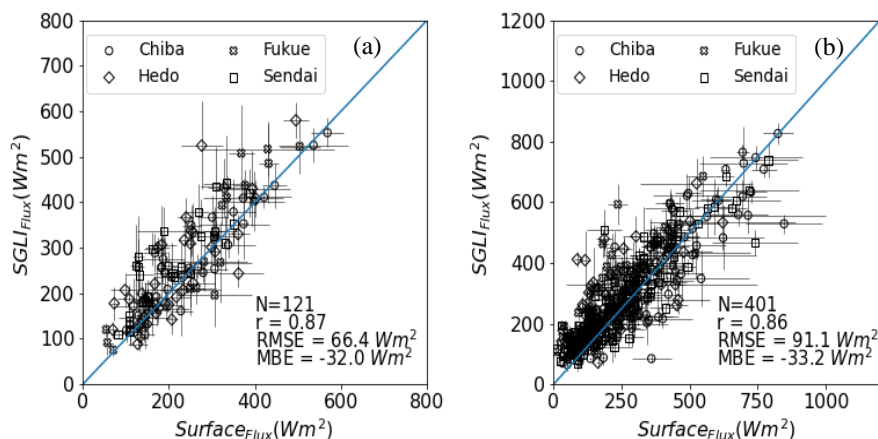
638

639

640

641

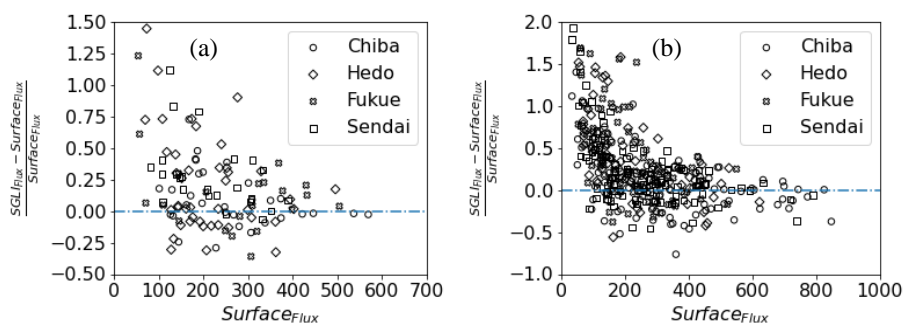
642



643

644 **Figure 9.** Comparison of surface-observed global irradiances with values modeled using SGLI-observed
 645 cloud properties for (a) water clouds and (b) ice clouds.

646



647

648 **Figure 10.** Scatter plots for modeled and observed global-irradiance difference and observed global
 649 irradiance for (a) water clouds and (b) ice clouds.